Journal of the American College of Cardiology 2009

DOI: 10.1016/j.jacc.2009.07.044

Bicuspid Aortic Valves with Different Spatial Orientations of the Leaflets Are Distinct Etiological Entities

Borja Fernández PHD,* Ana C. Durán PHD,* Teresa Fernández-Gallego BSC,* M. Carmen Fernández BSC,* Miguel Such MD† Josep M. Arqué MD,‡ Valentín Sans-Coma, PHD*

* Department of Animal Biology, Faculty of Science, University of Málaga, Málaga, Spain
† Department of Cardiovascular Surgery, University Hospital Virgen de la Victoria, Málaga, Spain
‡ Department of Cardiovascular Surgery, University Hospital Carlos Haya, Málaga, Spain.

Supported by grants SAF2006-01548 (Ministerio de Educación y Ciencia, Madrid, Spain), Beca para Investigación Básica en Cardiología (Spanish Society of Cardiology, Madrid, Spain), and Fondos Propios (University of Málaga, Málaga, Spain).

Objectives
The aim of this study was to decide whether bicuspid aortic valves (BAVs) with fused right and noncoronary leaflets (R-N) and BAVs with fused right and left leaflets (R-L) have different etiologies or are the product of a single diathesis.
Background
The BAV is the most common congenital cardiac malformation. The R-N and R-L BAVs are the most frequent BAV subtypes.
Methods
The study was carried out in adult and embryonic hearts of endothelium nitric oxide synthase knock-out mice and inbred Syrian hamsters with a high incidence of R-N and R-L BAVs, respectively. The techniques used were histochemistry, immunohistochemistry, and scanning electron microscopy.
Results
The R-N BAVs result from a defective development of the cardiac outflow tract (OT) endocardial cushions that generates a morphologically anomalous right leaflet. The left leaflet develops normally. The R-L BAVs are the outcome of an extrafusion of the septal and parietal OT ridges that thereby engenders a sole anterior leaflet. The noncoronary leaflet forms normally.

Conclusions

The R-N and R-L BAVs are different etiological entities. The R-N BAVs are the product of a morphogenetic defect that happens before the OT septation and that probably relies on an exacerbated nitric oxide–dependent epithelial-to-mesenchymal transformation. The R-L BAVs result from the anomalous septation of the proximal portion of the OT, likely caused by a distorted behavior of neural crest cells. Care should be taken in further work on BAV genetics because R-N and R-L BAVs might rely on different genotypes. Detailed screening for R-N and R-L BAVs should be performed for a better understanding of the relationships between these BAV morphologic phenotypes and other heart disease.

Key Words: bicuspid aortic valve, etiology, embryology, endothelial nitric oxide synthase, cardiac neural crest, animal models.

Abbreviations and Acronyms

BAV = bicuspid aortic valve
CoA = coarctation of the aorta
E/M = epithelial-to-mesenchymal
$eNOS^{-/-}$ = endothelium nitric oxide synthase knock-out
NC = neural crest
OT = outflow tract
R-L = right and left coronary leaflet
R-N = right and noncoronary leaflet
SM = smooth muscle

Bicuspid (bifoliate) aortic valve (BAV) is the most common congenital cardiac malformation (1). It may be silent during life; however, it entails a high risk of clinical complications, such as aortic stenosis and/or insufficiency, which usually require surgery (2,3). The BAV may appear as an isolated defect or associated with other congenital malformations, in particular coarctation of the aorta (CoA), interruption of the aortic arch, and ventricular septal defect (4,5). Moreover, patients with a congenital BAV often present dilation and dissection of the ascending aorta (reviewed in Fedak et al. 3).

The most frequent BAV subtypes are those with fusion of right and noncoronary leaflets (R-N) and those with fusion of right and left coronary leaflets (R-L) (6). Currently, it remains unknown whether they have different etiologies or result from a single diathesis. The present study was outlined to gain new insight into this question. It was carried out using endothelium nitric oxide synthase knock-out ($eNOS^{-/-}$) mice and inbred Syrian hamsters with a high incidence of BAVs (7,8).

METHODS

The $eNOS^{-/-}$ mice (B6.129P2-Nos3) were purchased from Jackson Laboratories (Bar Harbor, Maine) and genotyped by polymerase chain reaction as described previously (9). Syrian hamsters belonged to a family subjected to systematic inbreeding in our laboratory by mating siblings (7,10). The incidence of BAVs in the mutant mice and inbred hamsters amounts to 32% and 58%, respectively. Wild-type mice (C57BL/6J) and Syrian hamsters belonging to an inbred family with a low incidence (<2%) of BAVs served as control subjects.

The animals were handled in accordance with the international guidelines for animal welfare. Adult mice (n = 38) and hamsters (n = 142) were euthanized by carbon dioxide inhalation. Hearts were dissected, and the gross anatomy of the valves was assessed by a stereomicroscope. Embryos (43 mice, 86 hamsters) and adult hearts were fixed and cryopreserved, embedded in paraffin, or processed for scanning electron microscopy as described previously (9–11). Transverse and sagittal sections, 5 or 10 µm thick, were serially cut to alternate histochemical and immunoperoxidase stainings in consecutive sections. The staining methods were described elsewhere (9,10,12). The antibodies used were monoclonal anti-smooth muscle (SM) α-actin (Sigma-Aldrich, Madrid, Spain), polyclonal anti-tenascin (gift from Dr. M. Chiquet, Basel, Switzerland), and peroxidase-conjugated antimouse immunoglobulin G (Sigma-Aldrich).

RESULTS

Aortic valve morphology in adult $eNOS^{-/-}$ mice and Syrian hamsters. Before exposing our findings concerning BAVs, it should be noted that the normal aortic valve in both the mouse and the Syrian hamster is tricuspid (trifoliate). As in

humans, it consists of 3 aortic sinuses, right, left, and noncoronary, each supporting 1 leaflet (Figs. 1A to 1D).

Twelve (32%) of the 38 homozygote mutant mice possessed an R-N BAV (Figs. 1E and 1F). These defective valves had 2 aortic sinuses of similar size, and were devoid of any raphe. In all cases there were 2 coronary ostia. One of them was located in the aortic sinus that sustained the fused R-Ns. The other ostium was placed in the opposite aortic sinus.

Fifty (58%) of the 86 adult hamsters from the affected line showed an R-L BAV (Figs. 1G and 1H). Twenty-eight (56%) of the 50 BAVs had a raphe in the aortic sinus supporting the fused R-Ls (Fig. 2). In all R-L BAVs, the coronary ostia were located one in the right and the other in the left side of this aortic sinus.

Normal formation and division of the embryonic cardiac outflow tract (OT) in mice and hamsters. The normal formation and division (septation) of the single embryonic OT was similar in mice and hamsters. The OT appeared as a tubular myocardial structure, the luminal surface of which was furnished with 4 endocardial cushions, namely 2 OT ridges, septal and parietal, and 2 small intercalated cushions, anterior and posterior (Figs. 3, 4A, and 5A).

The OT septation started with the fusion of the central portions of the 2 ridges (Figs. 4B and 5B), followed by the development of the OT septum (Figs. 4C and 5C). The cells forming the septum, strongly reactive to SMα-actin antibodies (Figs. 6A and 7A), became organized in layers, using tenascin as a substrate adhesion protein (Fig. 7C). As a result of the septation process, the single embryonic OT became divided into the aortic and pulmonary OTs, each showing 3 valve cushions (Figs. 4C and 5C). The right and left aortic and pulmonary valve cushions developed from the nonfused margins of the 2 OT ridges, whereas the posterior (noncoronary) aortic and the anterior pulmonary valve cushions derived from the intercalated cushions (Figs. 4A to 4C and 5A to 5C).

Morphogenesis of R-N BAVs. Fourteen of the 43 mutant mouse embryos were at pre-septation stages; the fusion of the OT ridges had not started (Figs. 4A and 4D). In 4 (29%) of the 14 embryos, the parietal ridge and the anterior intercalated cushion were normal, whereas the septal ridge was abnormally fused with the posterior intercalated cushion (Fig. 4D; compare with Fig. 4A).

The other 29 mutant embryos were at diverse septation stages (Figs. 4B, 4C, 4E, and 4F). In 7 (24%) of these embryos, the developing OT septum, the pulmonary OT, and the myocardial wall showed no abnormality. However, the aortic OT showed only 2 cushions (Figs. 4E, 4F, and 6B), namely a normal left cushion, originated from the parietal ridge, and a right anomalous cushion, derived from the septal ridge and the posterior intercalated cushion (Figs. 4E and 4F; compare with Figs. 4B and 4C).

Morphogenesis of R-L BAVs. Twenty-four of the 86 inbred hamster embryos were at a pre-septation stage (Figs. 5A and 5D). All of them showed a normal morphology and distribution of the OT ridges and intercalated cushions.

The other 62 embryos were at diverse septation stages (Figs. 5B, 5C, 5E, and 5F). In 39 (63%) of them, the OT septation was altered (Figs. 5E and 5F). The fusion of the OT ridges was not confined to the center of the ridges; it involved their posterior margins, which normally conform to the primordia of the right and left aortic valve cushions (compare Figs. 5E and 5B). As a result of the extrafusion, a single anterior valve cushion developed at the aortic OT (Fig. 5F). In that case, the SM α-actin+ mesenchymal cells of the OT septum showed an anomalous distribution (Fig. 7B). They invaded the posterior margins of the extrafused area of the ridges, instead of remaining positioned symmetrically at the central portion of the ridges (compare Figs. 7B and 7A). Moreover, in the extrafused area, the cells of the resulting OT septum were disarranged (compare Figs. 5C and 5F), a fact that became more conspicuous when immunolabeling with antitenascin antibodies (compare Figs. 7C and 7D).

DISCUSSION

In humans, BAVs are thought to be the outcome of diverse etiologies (3,13,14). However, no empirical data support this notion. To our knowledge, the present embryological findings are the first to prove that R-N and R-L BAVs have different pathogenesis.

The observations in eNOS$^{-/-}$ mouse embryos indicate that R-N BAVs are the product of a defective formation of the embryonic OT endocardial cushions. Before the OT septation, the posterior margin of the septal ridge and the posterior intercalated cushion develop as a unique cushion, which is the anlagen of the anomalous right noncoronary aortic leaflet. The other leaflet develops from the left aortic cushion, derived from the normal parietal ridge. It must be stressed here that the formation of the OT septum is normal.

The observations in hamster embryos denote that R-L BAVs result from a defective OT septation. The septal and parietal OT ridges and the posterior intercalated cushion show a normal arrangement before the septation. However, the septation diverges from the normal pattern. The posterior margins of the ridges become extrafused, so that a single anterior cushion forms, from which the R-L fused aortic valve leaflet develops. The noncoronary leaflet derives from the normal posterior intercalated cushion.

The occurrence of BAVs in eNOS$^{-/-}$ mice was reported for the first time by Lee et al. (8). However, these investigators gave no information on the arrangement of the aortic leaflets and the embryology of these defective valves. Our observations show that they are R-N BAVs, and that their morphology becomes established before the OT septation. During normal cardiogenesis, eNOS expression is restricted to endocardial cells and is shear stress-dependent (15). Endothelium-derived nitric oxide is known to mediate endothelial cell podokinesis (16). The process of epithelial-to-mesenchymal (E/M) transformation, which is responsible for the colonization of the cardiac jelly by endocardial cells to form the endocardial

cushions, and which requires endocardial cell detachment and migration (17), is also shear stress-dependent. On this basis, it can be hypothesized that eNOS deficiency in mutant mice might alter endocardial cell migration during E/M transformation, leading thereby to an anomalous development of the valve cushions. Further support for this notion comes from the recent finding that in the kidney, experimental nitric oxide synthase inhibition promotes E/M transformation (18).

More than 10 years ago, we provided evidence that fusion of the right and left aortic valve cushions is a key factor in the formation of R-L BAVs with and without raphe (11). In addition, we suggested that an anomalous behavior of cardiac neural crest (NC) cells might be implicated in this event. Cell tracking experiments in avian and mammalian embryos have shown that NC cells migrate into the OT ridges and form the OT septum (19–22), using SMα-actin to generate the driving force (23) and tenascin as a substratum adhesion protein (24). The septum divides not only the aortic and pulmonary roots, but also the proximal parts of the developing OT, and seemingly the intrapericardial components of the arterial trunks (25,26). Taking into account that the septal component disappears in the definitive heart, the fate of the NC cells that participate in its formation remains unclear, although most recent data point to their disappearance (26,27). Another aspect that remains unclear is the specific mechanism by which the ridges become fused and the NC cells organize to form the OT septum (24,28). Our observations in hamster embryos indicate that in the formation of the R-L BAVs, the fusion of the OT ridges and the distribution of the septum cells are obviously distorted (Figs. 5 and 6). This reinforces the notion that altered NC behavior is responsible for the development of R-L BAVs.

We believe that there is enough evidence to decide that the R-N BAVs and the R-L BAVs are different etiological entities. The R-N BAVs are caused by a defective formation of the OT cushions, probably caused by an exacerbated nitric oxide-dependent E/M transformation. The R-L BAVs are the product of an anomalous embryonic OT septation, presumably produced by alterations in NC cell behavior.

A basic question is whether this conclusion can be extended to humans. In our opinion, this can be done because: 1) human, mouse, and hamster aortic valves are morphologically equivalent; and 2) the normal valve morphogenesis is similar in both rodent species and humans (19,29).

Recent studies devoted to the etiology of human BAVs indicate that genetic factors constitute almost certainly the primary cause of maldevelopment (13,14,30). Until now, however, family-based genome-wide linkage analyses were unable to identify the specific gene products responsible for BAV formation (13,30). In none of these genetic studies, R-N and R-L BAVs were regarded as dissimilar etiological entities. Our findings alert us that care should be taken in

further work concerning BAV genetics, given that R-N and R-L BAVs might rely on different genotypic variants.

The morphology of BAVs, that is, R-N versus R-L BAVs, is an important determinant of: 1) the risk of aortic stenosis and regurgitation (31); and 2) the elastic properties and dimensions of the aorta (32). It has been shown that patients with R-L BAVs have a more severe degree of aortic wall degeneration than patients with R-N BAVs (6), and that R-L BAVs, and not R-N BAVs, are significantly associated with CoA (31), a congenital malformation that is believed to be the outcome of a cardiac NC anomaly (4). Moreover, studies in children and adolescents have proven that R-N BAVs show a more rapid progression of aortic valve stenosis and regurgitation (31,33). These data, together with our findings, suggest that the etiological factors that determine the formation of R-N and R-L BAVs are also involved in the occurrence and progression of the pathologies associated with each BAV subtype. Detailed echocardiographic and surgical screenings for R-N and R-L BAVs should be performed to gain new insight on the relationships between these BAV subtypes and other heart disease.

Acknowledgments

The authors thank J. Moncayo for his contribution in obtaining the histological sections, G. Martín for assistance in electron microscopy, and L. Vida for technical assistance.

REFERENCES

1. Basso C, Boschello M, Perrone C, et al. An echocardiographic survey of primary school children for bicuspid aortic valve. Am J Cardiol 2004;93:661–3.

2. Edwards JE. The congenital bicuspid aortic valve. Circulation 1961; 23:485–8.

3. Fedak PWM, Verma S, David TE, Leask RL, Weisel RD, Butany J. Clinical and pathophysiological implications of a bicuspid aortic valve. Circulation 2002;106:900 – 4.

4. Kappetein AP, Gittenberger-de Groot AC, Zwinderman AH, Rohmer J, Poelmann RE, Huysmans HA. The neural crest as a possible pathogenetic factor in coarctation of the aorta and bicuspid aortic valve. Thorac Cardiovasc Surg 1991;102:830 – 6.

5. Durán AC, Frescura C, Sans-Coma V, Angelini A, Basso C, Thiene G. Bicuspid aortic valves in hearts with other congenital heart disease. J Heart Valve Dis 1995;4:581–90.

6. Russo CF, Cannata A, Lanfranconi M, Vitali E, Garatti A, Bonacina E. Is aortic wall degeneration related to bicuspid aortic valve anatomy with valvular disease? J Thorac Cardiovasc Surg 2008;136:937– 42.

7. Sans-Coma V, Arqué JM, Durán AC, Cardo M, Fernández B. Coronary artery anomalies and bicuspid aortic valves in the Syrian hamster. Basic Res Cardiol 1991;86:148 –53.
8. Lee TC, Zhao YD, Courtman DW, Stewart DJ. Abnormal aortic valve development in mice lacking endothelial nitric oxide synthase. Circulation 2000;101:2345– 8.
9. Fernández B, Buehler A, Wolfram S, et al. Transgenic myocardial overexpression of fibroblast growth factor-1 increases coronary density and branching. Circ Res 2000;87:207–13.
10. Sans-Coma V, Cardo M, Durán AC, et al. Evidence for quantitative genetic influence on the formation of aortic valves with 2 leaflets in the Syrian hamster. Cardiol Young 1993;3:132– 40.
11. Sans-Coma V, Fernández B, Durán AC, et al. Fusion of valve cushions as a key factor in the formation of congenital bicuspid aortic valves in Syrian hamsters. Anat Rec 1996;244:490 – 8.
12. Boengler K, Pipp F, Fernández B, Richter A, Schaper W, Deindl E. The ankyrin repeat containing SOCS box protein 5: a novel protein associated with arteriogenesis. Biochem Biophys Res Com 2003;302: 17–22.
13. Martin LJ, Ramachandran V, Cripe LH, et al. Evidence in favor of linkage to human chromosomal regions 18q, 5q and 13q for bicuspid aortic valve and associated cardiovascular malformations. Hum Genet 2007;121:275– 84.
14. Cripe L, Andelfinger G, Martin LJ, Shooner K, Benson DW. Bicuspid aortic valve is heritable. J Am Coll Cardiol 2004;44:138 – 43.
15. Groenendijk BCW, Hierck BP, Gittenberger-de Groot AC, Poelmann RE. Development-related changes in the expression of shear stress responsive genes KLF-2, ET-1, and NOS-3 in the developing cardiovascular system of chicken embryos. Develop Dyn 2004;230:57– 68.
16. Noiri E, Lee E, Testa J, et al. Podokinesis in endothelial cell migration: role of nitric oxide. Am J Physiol 1998;274:C236 – 44.
17. Hove JR, Koster RW, Forouhar AS, Acevedo-Bolton G, Fraser SE, Gharib M. Intracardiac fluid forces are an essential epigenetic factor for embryonic cardiogenesis. Nature 2003;421:172–7.
18. O'Riordan E, Mendelev N, Patschan S, et al. Chronic NOS inhibition activates endothelial-mesenchymal transformation. Am J Physiol Heart Circ Physiol 2007;292:H285–94.
19. Gittenberger-de Groot AC, Bartelings MM, DeRuiter MC, Poelmann RE. Basics of cardiac development for the understanding of congenital heart malformations. Pediatr Res 2005;57:169 –76.
20. Jiang X, Rowitch DH, Soriano P, McMahon AP, Sucov HM. Fate of the mammalian cardiac neural crest. Development 2000;127:1607–16.
21. Hutson MR, Kirby ML. Neural crest and cardiovascular development: a 20-year perspective. Birth Defects Res 2003;69:2–13.

22. Waldo KL, Lo CW, Kirby ML. Connexin 43 expression reflects neural crest patterns during cardiovascular development. Dev Biol 1999;208:307–23.

23. Beall AC, Rosenquist TH. Smooth muscle cells of neural crest origin form the aorticopulmonary septum in the avian embryo. Anat Rec 1990;226:360 – 6.
24. Hurle JM, Garcia-Martinez V, Ros MA. Immunofluorescent localization of tenascin during the morphogenesis of the outflow tract of the chick embryo heart. Anat Embryol 1990;181:149 –55.
25. Bradshaw L, Chaudhry B, Hildreth V, Webb S, Henderson DJ. Dual role for neural crest cells during outflow tract septation in the neural crest-deficient mutant Splotch2H. J Anat 2009;214:245–57.
26. Anderson RH, Webb S, Brown NA, Lamers W, Moorman A. Development of the heart: (3) formation of the ventricular outflow tracts, arterial valves, and intrapericardial arterial trunks. Heart 2005;89:1110 – 8.
27. Webb S, Qayyum SR, Anderson RH, Lamers WH, Richardson MK. Septation and separation within the outflow tract of the developing heart. J Anat 2003;202:327– 42.
28. Qayyum SR, Webb S, Anderson RH, Verbeek FJ, Brown NA, Richardson MK. Septation and valvar formation in the outflow tract of the embryonic chick heart. Anat Rec 2001;264:273– 83.
29. Maron BJ, Hutchins GM. The development of the semilunar valves in the human heart. Am J Pathol 1974;74:333– 44.
30. Hinton RB, Martin LJ, Rame-Gowda S, Tabangin ME, Cripe LH, Benson DW. Hypoplastic left heart syndrome links to chromosomes 10q and 6q and is genetically related to bicuspid aortic valve. J Am Coll Cardiol 2009;53:1065–71.
31. Fernandes SM, Sanders SP, Khairy P, et al. Morphology of bicuspid aortic valve in children and adolescents. J Am Coll Cardiol 2004;44: 1648 –51.
32. Schaefer BM, Lewin MB, Stout KK, Byers PH, Otto CM. Usefulness of bicuspid aortic valve phenotype to predict elastic properties of the ascending aorta. Am J Cardiol 2007;99:686 –90.
33. Fernandes SM, Khairy P, Sanders SP, Colan SD. Bicuspid aortic valve morphology and interventions in the young. J Am Coll Cardiol 2007;49:2211– 4.

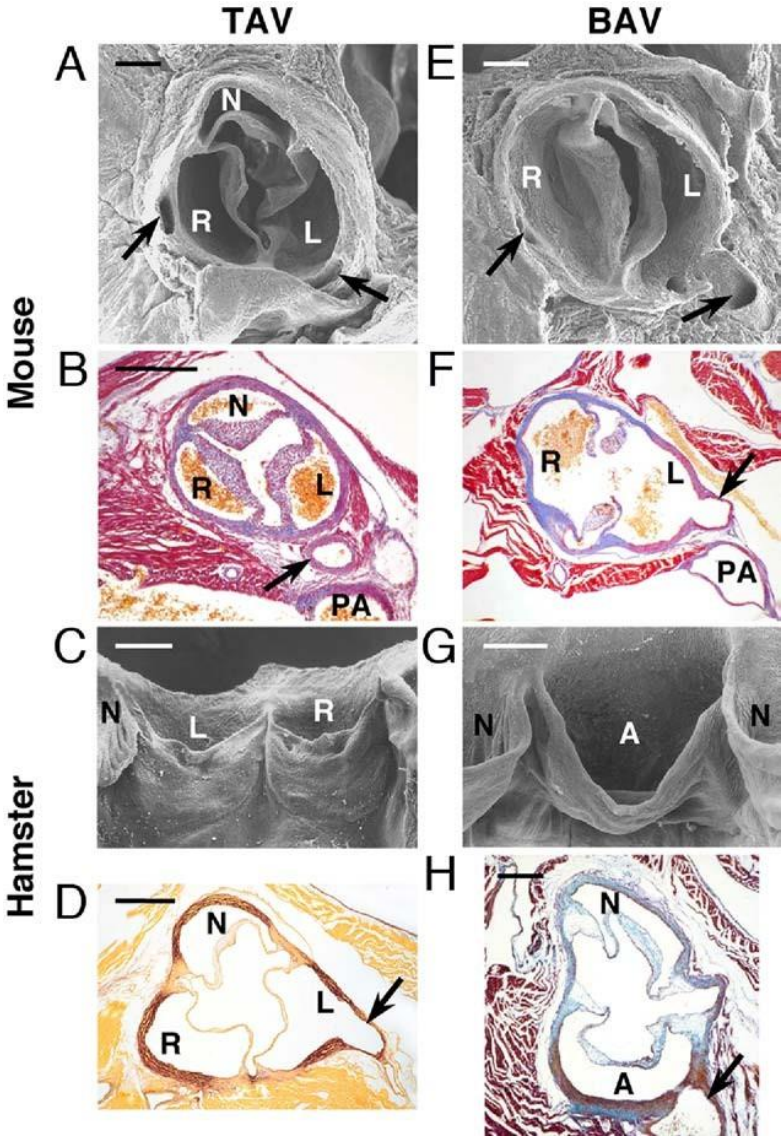

Figure 1 Aortic Valve Morphology

The tricuspid aortic valves (TAVs) (A to D) and bicuspid aortic valves (BAVs) (E to H) in endothelium nitric oxide synthase knock-out (eNOS-/-) mice (A, B, E, F) and inbred hamsters (C, D, G, H). Scanning electron micrographs. Cranial (A, E) and frontal (C, G) views. In (C) and (G), the specimens were opened through the noncoronary aortic sinus to show the anterior aspect of the valve. Transverse sections stained with Mallory trichrome (B, F), Masson-Goldner trichrome (H), and orcein-picrofuchsin (D) stains. The arrows point to the coronary arteries. In the mouse BAVs, R indicates the right aortic sinus supporting the fused right and noncoronary leaflets. Bars = 200 µm (A, B, E, F) and 400 µm (C, D, G, H). A = aortic sinus supporting the fused right and left coronary leaflets; L = left aortic sinus; N = noncoronary aortic sinus; PA = pulmonary artery; R = right aortic sinus.

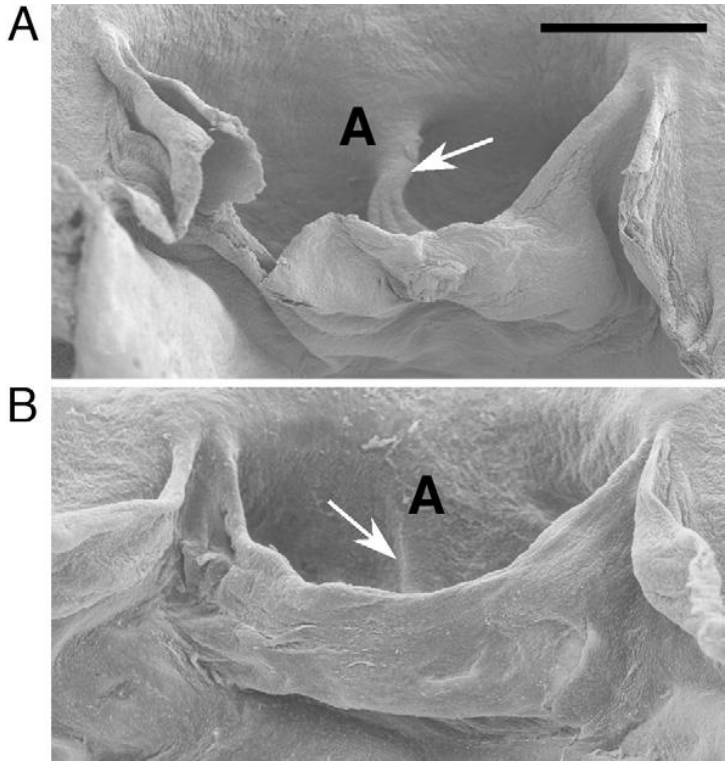

Figure 2 BAVs With Raphe from Inbred Hamster

Scanning electron micrographs, frontal views. The specimens were opened through the noncoronary aortic sinus to show the anterior aspect of the valve. (A) A BAV with a tall raphe (arrow) that contacts the anterior leaflet. (B) A BAV with a raphe (arrow) confined to the anterior sinus wall. Bar = 400 μm. Abbreviations as in Figure 1.

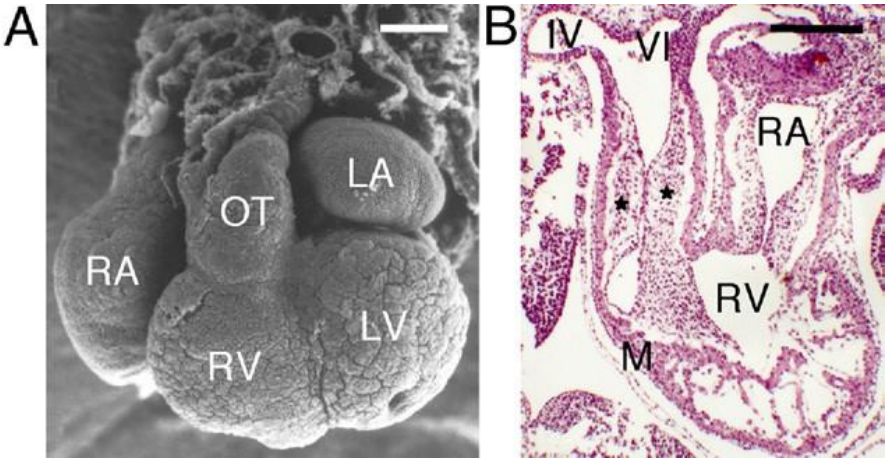

Figure 3 Normal Embryonic Ots of Hamster

Early stage of the OT septation. Embryos age 10.5 days post-coitum. (A) Scanning electron micrograph. (B) Sagittal section. Hematoxylin-eosin. Bar = 200 µm. *The 2 opposite OT ridges are arranged helicoidally. IV = fourth aortic arch; VI = sixth aortic arch; LA = left atrium; LV = left ventricle; M = myocardium; OT = outflow tract; RA = right atrium; RV = right ventricle.

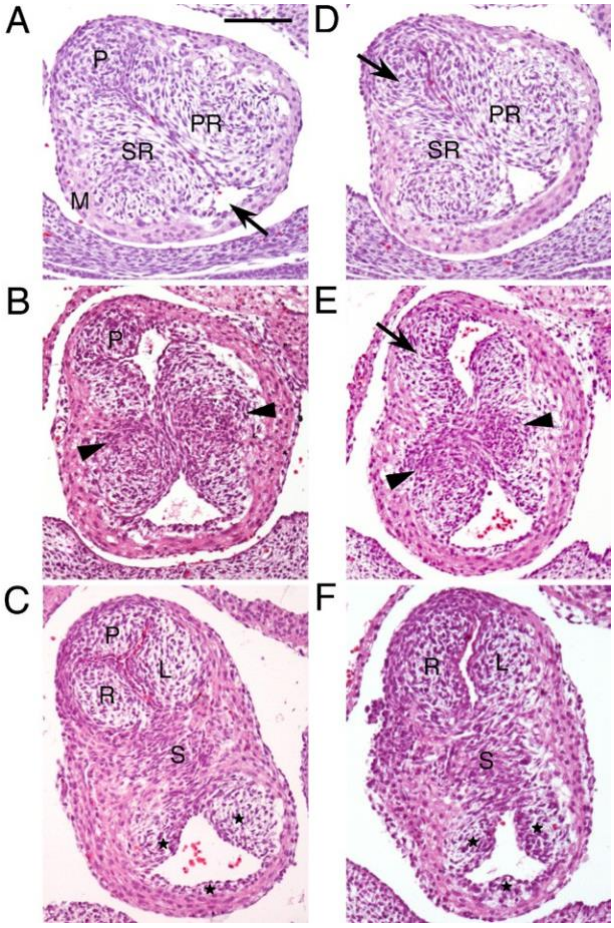

Figure 4 OT Septation in Mice

Transverse sections of the outflow tract (OT) before (A, D), during (B, E), and after (C, F) the OT septation. Embryos age 12 to 12.5 days post-coitum.

(A to C) Normal hearts. (D to F) Anomalous hearts. Hematoxylin-eosin. Bar = 100 µm. (A) Pre-septation. The septal ridge (SR) and parietal ridge (PR) are still independent. The anterior intercalated cushion is not visible because of the orientation of the section. The arrow points to its expected location. M = myocardium; P = posterior intercalated cushion. (B) Fusion of the SR and PR. Note that only the central portions of the ridges are fused. Arrowheads indicate OT septum anlagen. P = posterior intercalated cushion. (C) Formation of the OT septum (S). The septum divides the OT into an aortic (upper left) and a pulmonary (lower right) channel. *Pulmonary valve cushions. L = left aortic valve cushion; P = posterior (noncoronary) aortic valve cushion; R = right aortic valve cushion. (D) The SR and PR face each other as in the control (normal) specimens (compare with A). However, the posterior intercalated cushion is fused (arrow) to the septal ridge. (E) The central portions of the septal and parietal OT ridges are fused. The posterior intercalated cushion is abnormally fused (arrow) with the septal ridge. Arrowheads indicate OT anlagen. (F) After the OT septation, only 2 aortic valve cushions, right (R) and left (L), and 3 pulmonary valve cushions (*) are present. The OT septum (S) is normal.

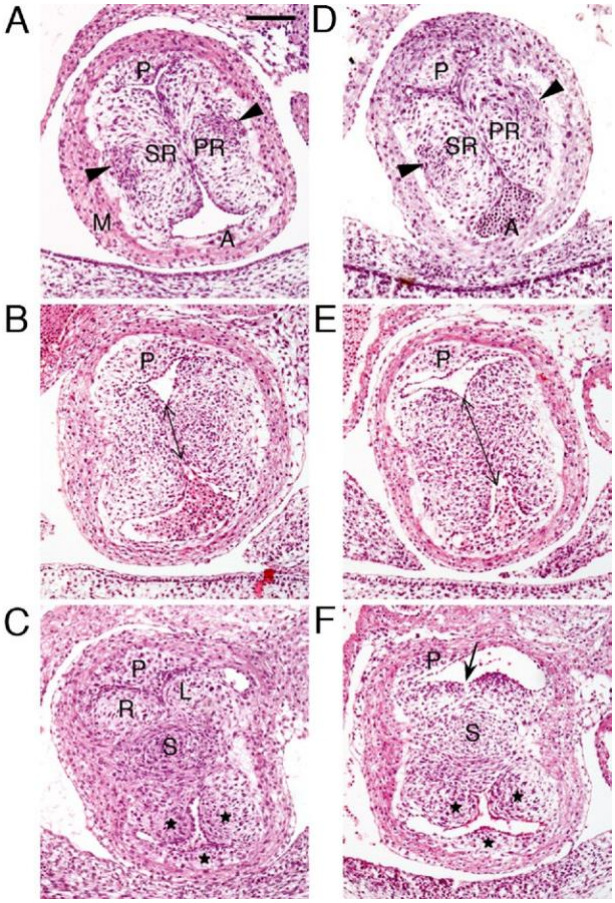

Figure 5 OT Septation in Hamster

Transverse sections of the OT before (A and D), during (B and E), and after (C and F) the OT septation. Embryos age 11 to 12 days post-coitum. (A to C) Control line. (D to F) Affected line. Hematoxylin-eosin. Bar = 100 µm. (A) The OT septum anlagen consists of 2 cellular condensations (arrowheads), located at the center of the SR and PR, close to the myocardium (M). P = posterior intercalated cushion. (B) Fusion of the OT ridges. The double-headed arrow delimits the normal extension of the fusion. P = posterior intercalated cushion. (C) Formation of the OT septum (S). The developing septum is composed of cell layers arranged concentrically. L = left aortic valve cushion; P = posterior (noncoronary) aortic valve cushion; R = right aortic valve cushion. (D) The SR and PR and the cellular condensations of the OT septum anlagen (arrowheads) are similar to those of control hamsters (compare with A). P = posterior intercalated cushion. (E) The fusion of the OT ridges (double-headed arrow) extends much more than usual toward the posterior margins of the ridges (compare with B). P = posterior intercalated cushion. (F) The right and left aortic valve cushions are extensively fused (arrow). The layers of cells of the OT septum (S) are less condensed than in the normal embryos (compare with C). P = posterior (noncoronary) aortic valve cushion. *Pulmonary valve cushions. A = anterior intercalated cushion.

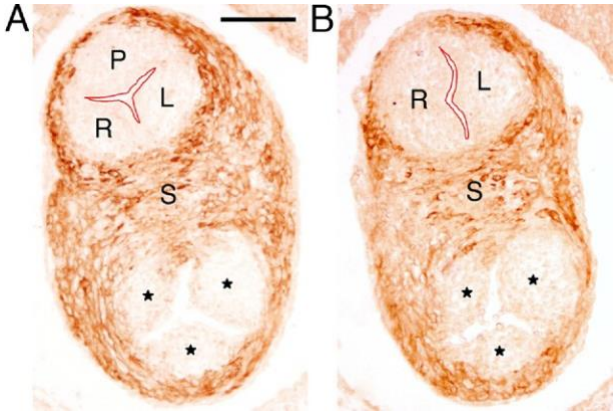

Figure 6 The OT Septum in Mice

Immunolocalization of smooth muscle (SM) α-actin in the embryonic outflow tract (OT). The contour of the endocardium of the aortic valve cushions (red) is outlined. Bar = 100 µm. (A) Consecutive section to that shown in Figure 4C. Normal embryo. (B) Consecutive section to that shown in Figure 4F. Embryo developing a bicuspid aortic valve with fused right and noncoronary leaflets.

Note that the OT septum (S) shows no alteration. *Pulmonary valve cushions. L = left aortic valve cushion; P = posterior (noncoronary) aortic valve cushion; R = right aortic valve cushion derived from the septal ridge and the posterior intercalated cushion.

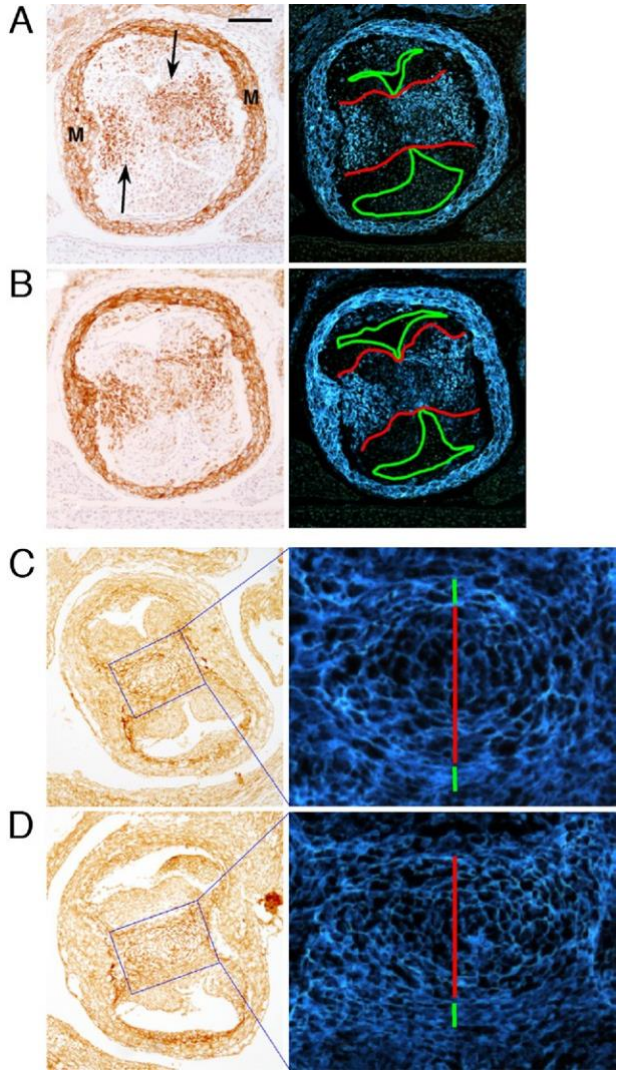

Figure 7 The OT Septum of Hmasters

Immunolocalization of SMα-actin (A, B) and tenascin (C, D) in the embryonic OT. (Left) Immunoperoxidase labeling (brown). (Right) The same pictures, but color-inverted using NIH Image software version 1.62 (National Institutes of Health, Bethesda, Maryland). (C, D) Close-up view. Bar = 100 µm. (A) Consecutive section to that shown in Figure 5B. (Left) The myocardium (M) and the cells forming the OT septum (arrows) are SMα-actin+; the latter invade the territory where the OT ridges fuse. (Right) The contour of the endocardium (green) and the extension of the septum cells (red) are outlined. (B) Consecutive section to that shown in Figure 5 E. In this anomalous specimen, the SMα-actin+ cells of the OT septum expand their distribution toward the posterior margins of the ridges, which results in an asymmetrical arrangement of the septum cells (compare the red lines in B with those in panel A). (C) Consecutive section to that shown in Figure 5C. (Left) Tenascin concentrates in both the myocardium/mesenchyme limit and the layers of the OT septum (rectangle). (Right) The color-inverted close up shows the distribution of tenascin around the core of the septum. The red and green lines indicate the central and peripheral (concentric cell layers) zones of tenascin distribution, respectively. (D) Consecutive section to that shown in Figure 5F. (Left) Note the different distribution of tenascin in the portion of the OT septum (rectangle) facing the aortic tract (top) compared with that facing the pulmonary tract (bottom). (Right) The OT septum is asymmetric because of the reduced tenascin deposition in the posterior peripheral layers of the septum (compare the red and green lines in D with those in C).